International Journal of Physical Sciences Vol. 7(11), pp. 1746 – 1761, 9 March, 2012
Available online at http://www.academicjournals.org/IJPS
DOI: 10.5897/IJPS11.1746
ISSN 1992 - 1950 ©2012 Academic Journals

Full Length Research Paper

Nonlinear dynamic analysis and chaos control for third order sub-harmonic in a ferroresonant circuit

Yanping Wu and Guodong Wang*

Department of Physics, Northwest A&F University, Yangling Shaanxi 712100, China.

Accepted 08 February, 2012

In this paper, the nonlinear dynamics of a non-autonomous system model for third order sub-harmonic in a basic ferroresonant circuit are analyzed in details, including phase trajectory, Poincaré map, bifurcation diagram, dissipativity analysis and Spectrogram map. Furthermore, a sliding mode controller of the system is designed and both theory analysis and numerical simulation are presented, which shows the effectiveness and potentials of the proposed techniques.

Key words: Third order sub-harmonic model, dynamics analysis, sliding mode control.

INTRODUCTION

Chaos theory is a very interesting phenomenon which has provided us a new way of viewing the universe and is an important tool to understand the world we live in. Chaotic behaviors are useful in many real-world applications such as secure communication (Khadra et al., 2005), mathematics (Liu and Yang, 2010), time series (Zhang and Small, 2006), biology (Ma et al., 2009; Zhang et al., 2010), circuit (Chen et al., 2012), human brain dynamics (Schiff et al., 1994), and heart beat regulation (Brandt and Chen, 1997), and so on.

The ferroresonance is a nonlinear resonance phenomenon that can affect the electrical transmission and distribution networks (Jacobson et al., 2002; Wornle et al., 2005). The analyzed circuit is a simplest physical model of large electrical power system in which forroresonant oscillation can occur and this is shown in Figure 1. Although, apparently simple, it indicates all oscillating phenomena, generally periodic, which particularly appear on all networks at capacitive dominant in interaction (Lamba et al., 1998; Preetham et al., 2006; Wornle et al., 2005; Lind et al., 2006). Some authors who attempt to study ferroresonance were reported in Preetham et al. (2006) and Saravanaselvan and Ramanujam (2011). In Milicevic et al. (2008, 2009), the authors presented a measurement system for model verification of non autonomous second-order nonlinear systems and predicted the prechaotic birfurcation points of a ferroresonant circuit. The chaotic behaviour exhibited by a typical ferroresonant circuit in a neutral grounding system is investigated in Hui et al. (2009). The article Ben Amar and Dhifaoui (2011) study the periodic ferroresonance in the electrical power networks by bifurcation diagrams.

As the chaotic state in most systems is harmful, thus chaos control is of great help. Chaos control is disquisitive in how to control the chaotic system to the periodic orbit or equilibrium point with the original parameters remained or only fine-tuned when the system parameters cannot be changed objectively, or the parameters change largely must pay a great price. Typical control methods have been proposed to achieve chaos control. Based on Ott, Grebogi, Yorke (OGY) approach, a multiparameter semi-continuous method was designed to control chaotic behavior in Paula de and Savi (2009) work. The unified chaotic systems with uncertain parameters were synchronized based on the control Lyapunov function (CLF) method in Wang et al. (2009). In Chen et al. (2011a, b) proposed a sliding mode control and its no-chattering method with uncertain parameters and bounded external disturbances to control chaotic system. Furthermore, in Shi et al. (2006), considering the problems of stochastic stability and sliding-mode control for a class of linear continuous-time systems with stochastic jumps, a reaching motion controller is designed such that the resulting closed-loop system can be driven onto the desired sliding surface in a limited time. In Yokoi and Hikihara (2011), a control method was

*Corresponding author. E-mail: gd.wang@yahoo.cn or wuyanping1993@126.com

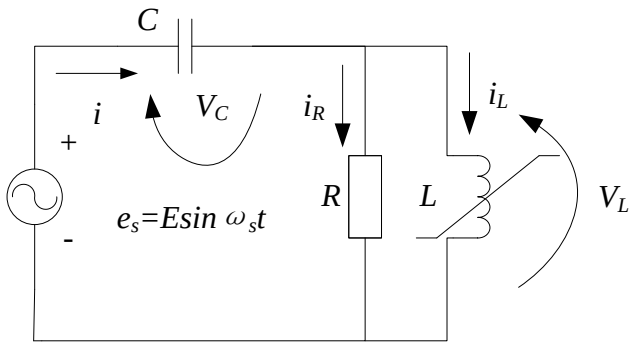

Figure 1. Basic ferroresonant circuit.

proposed for establishing periodic rotation inherent in parametric pendulum based on a delayed feedback control. In another related work Henning et al. (2011), the authors used dynamical barriers to control the transmission of light through slowly varying photonic crystals. Wang et al. (2011) designed a novel nonfragile linear state feedback controller to realize the mixed outer synchronization (MOS) between two networks and proved analytically by using Lyapunov-Krasovskii stability theory.

Motivated by all the current discussion, there are several advantages which make our approach attractive, compared with previous works. First, the nonlinear dynamics behaviors of a non-autonomous system model are analyzed for various values of the parameters using Poincaré maps, bifurcation diagrams, and the power spectrum. Moreover, we present a sliding mode control method with only one controlling term for the system, in which saturation function is substituted for sign function. The control method introduces an adaptive law with dead zone, while the adaptive rate also has some nonlinear characters.

SYSTEM DESCRIPTION AND AVERAGING

Here, the system equations along with a brief outline of the averaging method are presented. In the circuit, shown in Figure 1, the nonlinear inductor and the parallel resistor (*R*) represent the transformer. It is to be noted that the magnitude of the iron core losses which consists of (*a*) hysteresis losses and (*b*) eddy current losses, depend both on the flux density as well as the supply frequency. While modeling this dependence may be useful in creating a more accurate core loss model, here, the losses are aggregated and represented by a resistor *R* for simplicity of analysis. The nonlinearity of the core is modeled by the following equation.

$$i_M = a\lambda + b\lambda^n \tag{1}$$

The capacitor *C* represents the coupling effect between the source voltage at a supply frequency of ω_s. The supply voltage $e(t)$ is given by $e(t)=V_s\cos(\omega_s t)$. Then the dynamics of the circuit in Figure 1 can be described by the following equation.

$$\ddot{\lambda} + k\dot{\lambda} + a_1\lambda + b_1\lambda^n = G\cos(\omega_s t) \tag{2}$$

Where, $k=\frac{1}{RC}$, $a_1=\frac{a}{C}$, $b_1=\frac{b}{C}$, and $G=V_s\omega_s$. When the index *n* of the magnetization curve is three, Equation 2 is functionally similar to the periodically forced Duffing oscillator.

Remark 1

In the context of ferroresonance, the index *n* is usually obtained by approximating the magnetizing characteristics by a two term polynomial of suitable order. In Jacobson et al. (2002) and Mozaffari et al. (1995), indices corresponding to *n=3* and 13 were used in the calculations. Jacobson et al. (2002) examined the effect of the index *n* on ferroresonant oscillations and lower exponents were found satisfactory in representing small capacity transformers. In this paper, the index *n* is set to three for ease and tractability of the analysis. Thus, (2) with *n=3* is used to determine analytically the regions in 2D parameter space (V, V_s), where sub-harmonic resonance can persist.

Detailed analysis has been done on the Duffing oscillator since the classical work of Duffing. In particular, primary resonance, third order sub-harmonic and super-harmonic resonances have been exhaustively studied in the classical texts of (Nayfeh, 1981, 1979) by using perturbation techniques such as the methods of averaging and multiple scales. A brief outline of the averaging method to analyze third order sub-harmonic resonance is provided here. The classic Duffing equation is provided here. The classic Duffing equation is described by

$$\frac{d^2u}{dt^2} + k_1u + k_3u^3 = F\cos(\omega_s t) \tag{3}$$

After a suitable amplitude and time scaling (Nayfeh, 1979), the dimensionless form of the Duffing equation including the effect of a small viscous damping can be expressed as

$$\ddot{v} + \omega_0^2 v + 2\varepsilon\mu\dot{v} + \alpha\varepsilon v^3 = F\cos(\omega t) \tag{4}$$

The averaging method starts by noting that when $\varepsilon \in 0$, the general solution to (4) is given by

$$v = A\cos(\omega_0 t + \beta) + 2\Gamma\cos(\omega_s t) \tag{5}$$

where $\Gamma=\frac{F(\omega_0^2-\omega^2)^{-1}}{2}$, $\varepsilon \neq 0$, the solution is still represented

in the same form as in Equation 5, except that now the variables A and β are treated as time varying instead of constant. Thus, replacing A by A(t) and β by β(t) in Equation 5, the derivatives $\ddot{v}$ and $\dot{v}$ are computed and substituted in Equation 4 to solve for A(t) and β(t). It can be shown (Nayfeh, 1981) that resonant conditions arise in the system when

$\omega = \omega_0$ termed as fundamental frequency, or period-1 ferroresonance (Jacobson et al., 2002).
$3\omega = \omega_0$ termed as superharmonic resonance.
$\omega = 3\omega_0$ termed as sub-harmonic resonance (which is the subject of this paper).
$\omega = 0$ which is not of relevance to ferroresonance.

For the case $\omega = \frac{\omega_0}{3}$, following the development in Nayfeh (1981), the averaged equations for the system in Equations 2 can be written as

$$\dot{A} = -\frac{kA}{2} - \frac{3b_1 \Gamma A^2 \sin(\beta)}{4\omega_0} \tag{6}$$

$$\dot{\beta} = (\omega_f - 3\omega_0) - \frac{9b_1}{\omega_0}[\Gamma^2 - \frac{A^2}{8} - \frac{\gamma A \cos(\beta)}{4}] \tag{7}$$

where $\omega_0^2 = a_1 = \frac{a}{C}$, $\Gamma = \frac{G(\omega_0^2 - \omega_s^2)}{2}$. Setting the right hand side of Equations 6 and 7 to zero yields the steady state amplitude and phase of the sub-harmonic oscillations described by

$$\frac{-kA}{2} = \frac{3b_1 \Gamma A^2 \sin(\beta)}{4\omega_0} \tag{8}$$

$$(\omega_s - 3\omega_0) = \frac{9b_1(\Gamma^2 - A^2)}{\omega_0(8 - \frac{\gamma A \cos(\beta)}{4})} \tag{9}$$

For a nontrivial sub-harmonic oscillation to exist, it is evident that $A > 0$. Eliminating b from Equations 8 and 9, one can arrive at a quadratic in A^2 and derive a condition (Nayfeh, 1981) for the existence of nontrivial sub-harmonic oscillations, the result of which is described by

$$\frac{63b_1 G^2}{8\omega_0 k(\omega_0^2 - \omega_s^2)} = \frac{2(\omega - 3\omega_0)}{k} \pm \sqrt{\frac{4(\omega - 3\omega_0)2}{k^2} - 63} \tag{10}$$

The condition described in Equation 10 defines the boundary of the region where sub-harmonic oscillations can exist. In this paper, the parameters of interest in Equations 10 are (i) the coupling capacitance C, which decides the natural frequency of oscillation ω_0, (ii) the amplitude of the source voltage V_s and (iii) the core loss resistor R. The dependence of the sub-harmonic domains on the parameters of interest and consequently, its implications to ferroresonance is thus discussed. The system mode of Equation 2 is described as follows

$$\begin{cases} \frac{dx}{dt} = y \\ \frac{dy}{dt} = -\frac{1}{RC}y - \frac{a}{C}x - \frac{b}{C}x^3 + V_s\omega_s \cos(\omega_s t) \end{cases} \tag{11}$$

Where define $x = \lambda$, $y = \frac{dx}{dt}$.

SYSTEM DYNAMICS ANALYSIS

In this study, the nonlinear dynamics of the system are analyzed using dynamic trajectory, Poincaré map, bifurcation diagram, dissipativity analysis and spectrogram map. The basic principles and numerical results of each analytical method are reviewed in the following below.

The dynamic trajectories of the system provide a basic indication as to whether the system behavior is periodic or non-periodic. The numerical simulations of Equation 11 with several different parameters show that the dynamic trajectories are non-periodic.

The dynamic trajectories of the system are unable to identify the onset of chaotic motion. Accordingly, some other form of analytical method is required. In the present study, define $\theta = \omega_s t$, and Equation 11 is rewritten as follows

$$\begin{cases} \frac{dx}{dt} = y \\ \frac{dy}{dt} = -\frac{1}{RC}y - \frac{a}{C}x - \frac{b}{C}x^3 + V_s\omega_s \cos(\theta) \\ \frac{d\theta}{dt} = \omega_s \end{cases} \tag{12}$$

Obviously, Equation 11 is a non-autonomous system, while Equation 12 is autonomous. The dynamics of Equation 12 are analyzed using Poincaré maps derived from the Poincaré section of the systems. A Poincaré section is a hyper-surface in the state-space transverse to the flow of the system of interest. The projections of the Poincaré section on the x plane and the y plane are referred to as the Poincaré map of the dynamic system.

Table 1. Different values of R, C, V_s and ω_s and negative values of exponential rate p.

R(KΩ)	C(μF)	V_s(p.u)	ω_s(p.u)	p
10	4.1	1	1	-0.0244
10	7.2	1	1	-0.0139
10	13.5	1	1	-0.0074
10	6.7	2	1	-0.0149
10	12.7	2	1	-0.0079
10	22	2	1	-0.0045
10	18	3	1	-0.0056

When the system performs quasi-periodic motion, the return points in the Poincaré map form a closed curve. For chaotic motion, the return points form a fractal structure comprising many irregularly-distributed points. In the numerical simulation, the Poincaré maps of Equation 12 show chaotic motion.

A bifurcation diagram summarizes the essential dynamics of a system and is therefore a useful means of observing its nonlinear dynamic response. In the present analysis, rewrite the Equation 11 as:

$$\begin{cases} \dfrac{dx}{dt} = y \\ \dfrac{dy}{dt} = -ky - a_1 x - b_1 x^3 + \omega_s V_s \cos(\omega_s t) \end{cases} \tag{13}$$

The bifurcation diagrams are generated using k as the control parameter. In this case, the bifurcation control parameter is varied with a constant step and the state variables at the end of one integration step are taken as the initial values for the next step. In the numerical simulation, the corresponding variations of the x coordinate and y coordinate of the return points in the Poincaré maps of Equation 12 are plotted to form the bifurcation diagrams.

For Equation 11 with R=10KΩ, C=4.1μF, V_s=1p.u, ω_s=1p.u, we can obtain

$$\nabla V_1 = \frac{\partial \dot{x}}{x} + \frac{\partial \dot{y}}{y} = 0 - 0.0244 = -0.0244 = p$$

Where, p is a negative constant. Thus, Equation 11 is a dissipative system.

$$\frac{dV}{dt} = e^{p} = e^{-0.0244}$$

For Equation 11, a volume element V_0 is apparently contracted by the flow into a volume element $V_o e^{pt} = V_o e^{-0.0244t}$ in time t. It means that each volume containing the trajectory of this dynamical system shrinks to zero as $t \to \infty$ at an exponential rate p. Thus, all these dynamical systems orbits are eventually confined to a specific subset that have zero volume, and the asymptotic motion settles on an attractor of the systems.

For different values of the parameters R, C, V_s and ω_s, the values of p is also a negative constant.

Power spectrum of chaotic system exhibits continuous broadband feature. The numerical simulation for power spectrum of Equation 11 exhibits continuous broadband feature.

The simulation results are carried out using the MATLAB software with initial value $[x\ y]^T=[0.5\ 0.8]^T$. The sampled data of the parameters R, C, V_s and ω_s shown in Table 1 was used to generate the dynamic trajectories, Poincaré maps, bifurcation diagrams and power spectrum of the system in order to obtain a basic understanding of its dynamic behavior and identify the onset of chaotic motion. Figures 2, 3, 4, 5, 6, 7 and 8 represent the dynamic behaviors of Equation 11 with different values of parameters R, C, V_s and ω_s**.**

SLIDING MODE CONTROL AND SIMULATION RESULTS

Controller design

The controlled form of the Equation 11 is defined as:

$$\begin{cases} \dfrac{dx}{dt} = y \\ \dfrac{dy}{dt} = f(t,[x,y]^T) + u = p_1 y + p_2 x + p_3 x^3 + V_s \omega_s \cos(\omega_s t) + u \end{cases} \tag{14}$$

It is noted that the controller is active just when the current-driven induction motor system starts, that is, in chaotic state. But it is not active at other times.

Here, to make Equation 14 track the aim orbit x_d, which is n-order differentiable, we give a controller designed as follows:

$$\begin{aligned} u &= -f(t,[x,y]^T) + x_d^{(2)} + \sum_{i=1}^{2} c_i e^{(2-i)} + \int_0^t rsat(\frac{S}{\varepsilon})dt + m\int_0^t rsdt \\ &= -p_1 y - p_2 x - p_3 x^3 - V_s \omega_s \cos(\omega_s t) + x_d^{(2)} + \sum_{i=1}^{2} c_i e^{(2-i)} + \int_0^t rsat(\frac{S}{\varepsilon})dt + m\int_0^t rsdt \end{aligned} \tag{15}$$

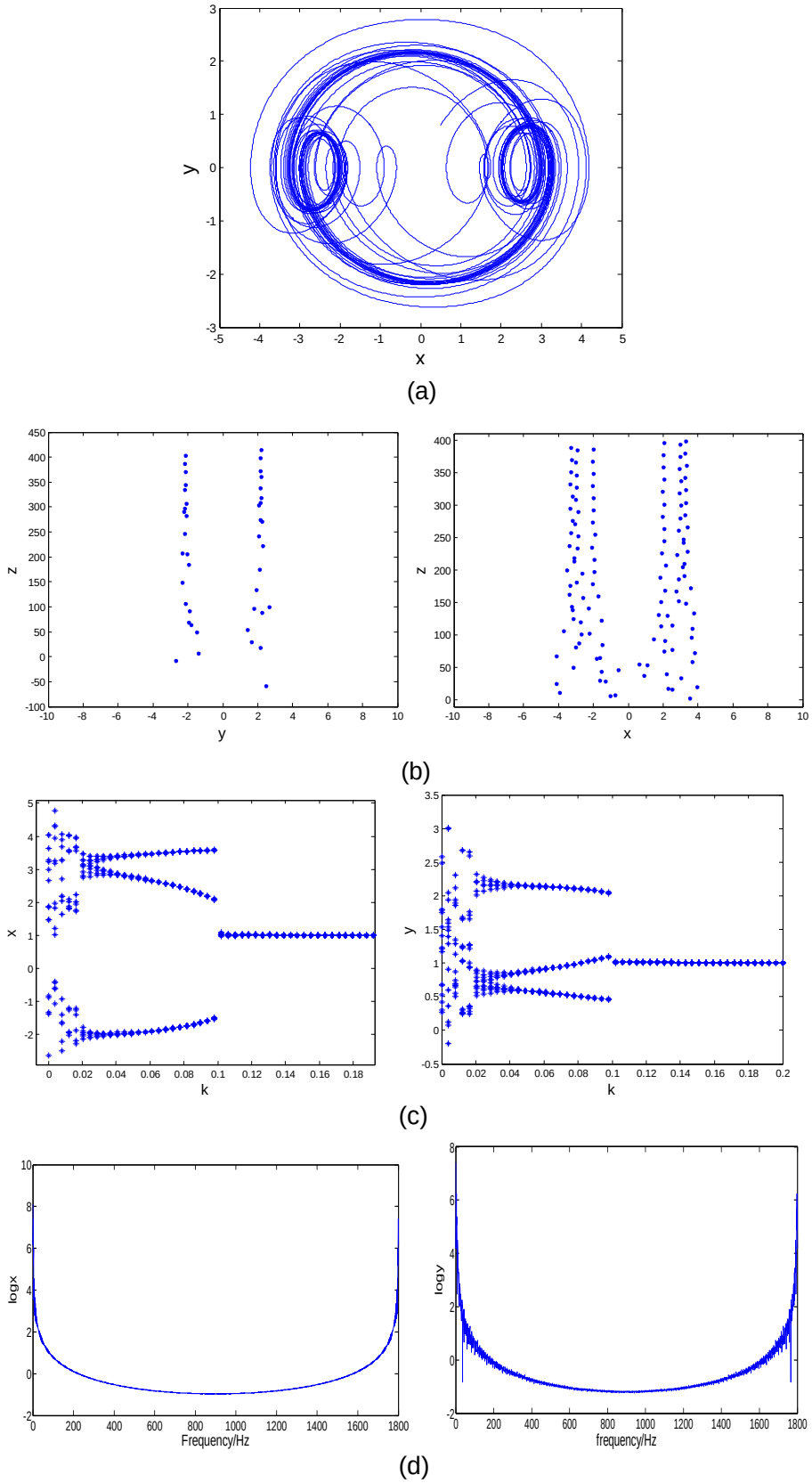

Figure 2. Simulation result obtained for Equation 11 with R=10KΩ, C=4.1μF, V_s=1p.u, ω_s=1p.u; (a) Dynamic trajectories (x-y) (b) Poincaré maps (c) Bifurcation maps w.r.t k (d) power spectrum: *logx-frequency/Hz* and *logy-frequency/Hz*.

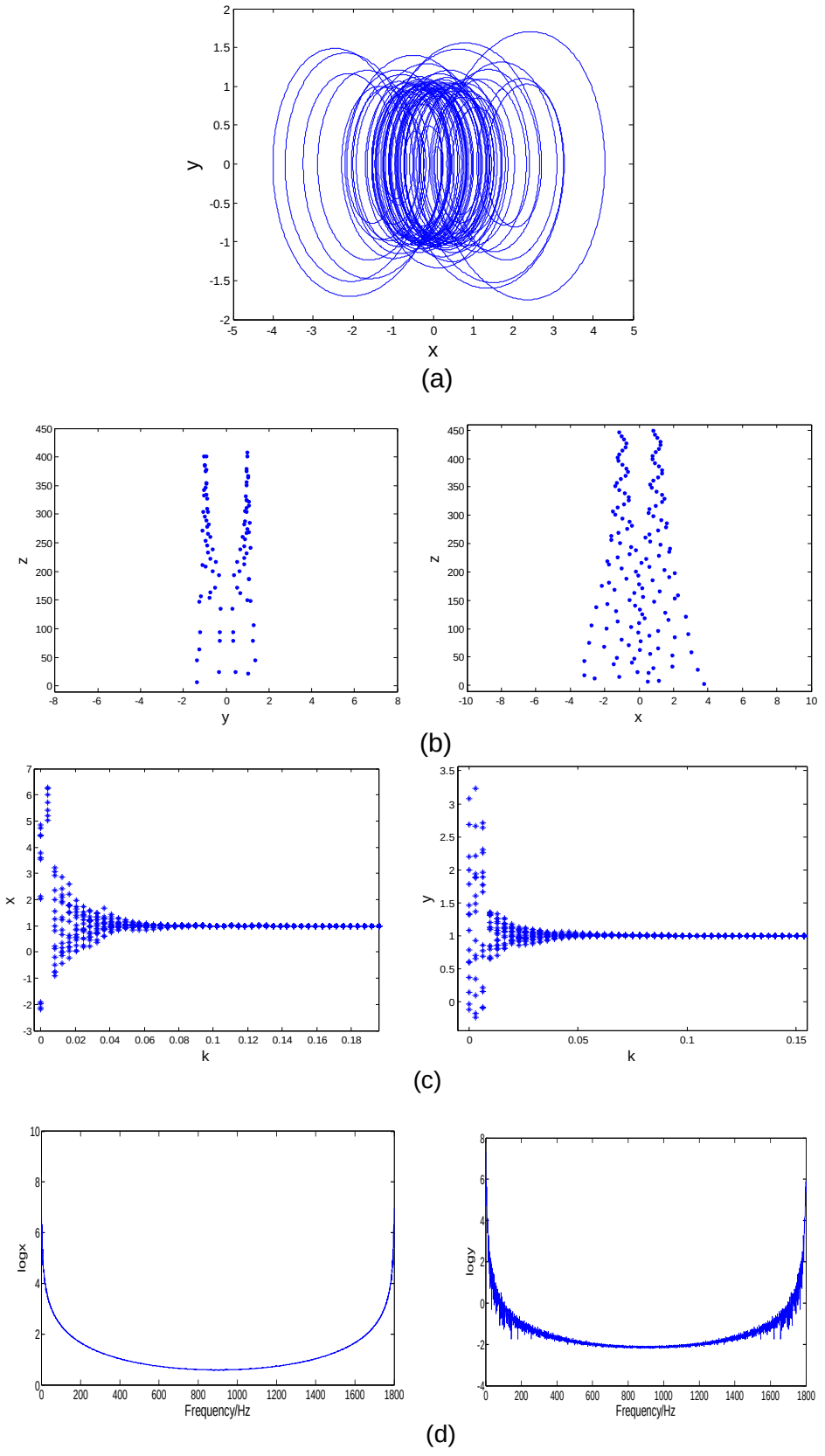

Figure 3. Simulation result obtained for Equation 11 with R=10KΩ, C=7.2μF, V_S=1p.u, ω_S=1p.u; (a) dynamic trajectories (x-y) (b) Poincaré maps (c) bifurcation maps w.r.t k (d) power spectrum: *logx-frequency/Hz* and *logy-frequency/Hz*.

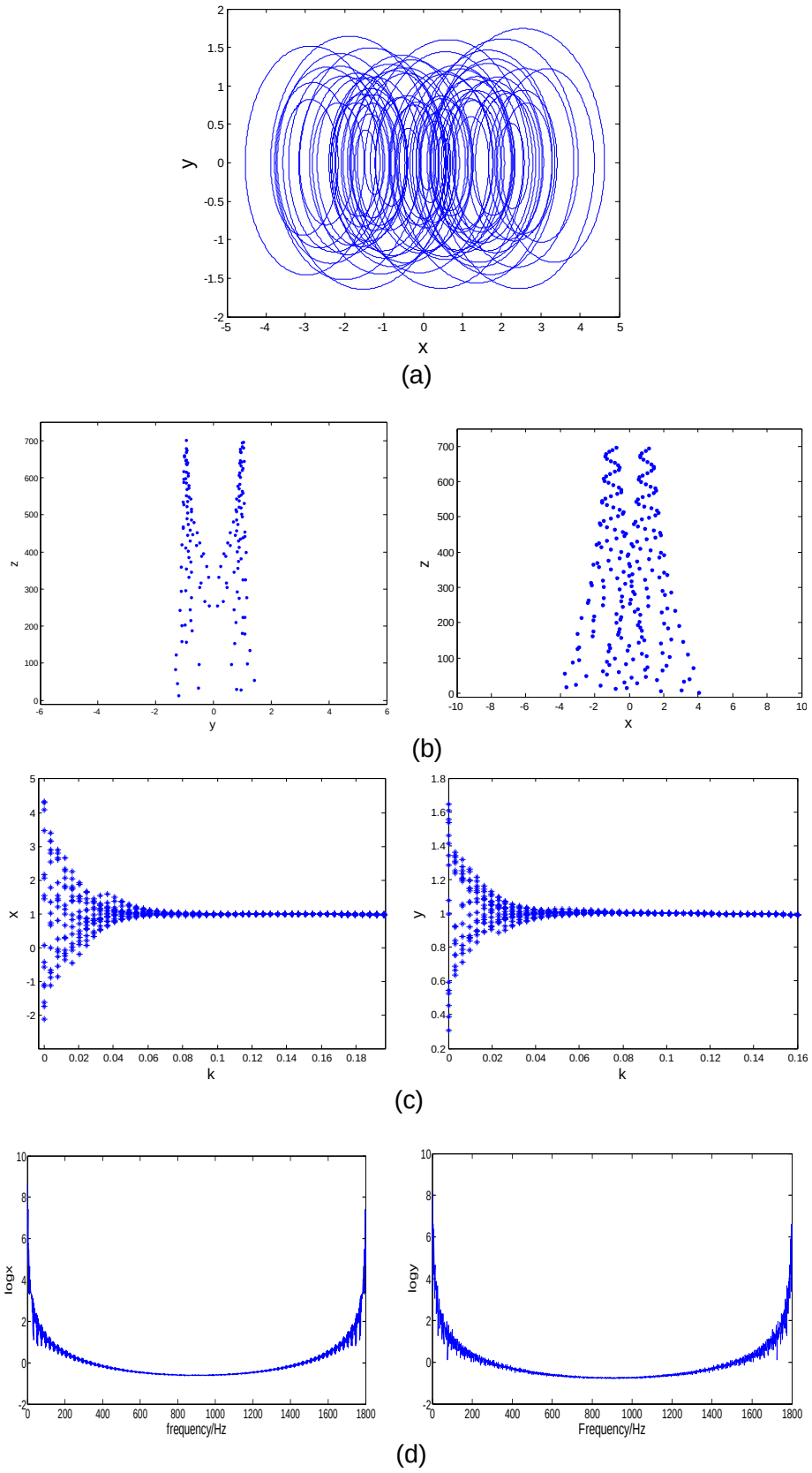

Figure 4. Simulation result obtained for Equation 11 with R=10KΩ, C=13.5μF, V_s=1p.u, ω_s=1p.u; (a) Dynamic trajectories (x-y) (b) Poincaré maps (c) bifurcation maps w.r.t k, (d) power spectrum: *logx-frequency/Hz* and *logy-frequency/Hz*.

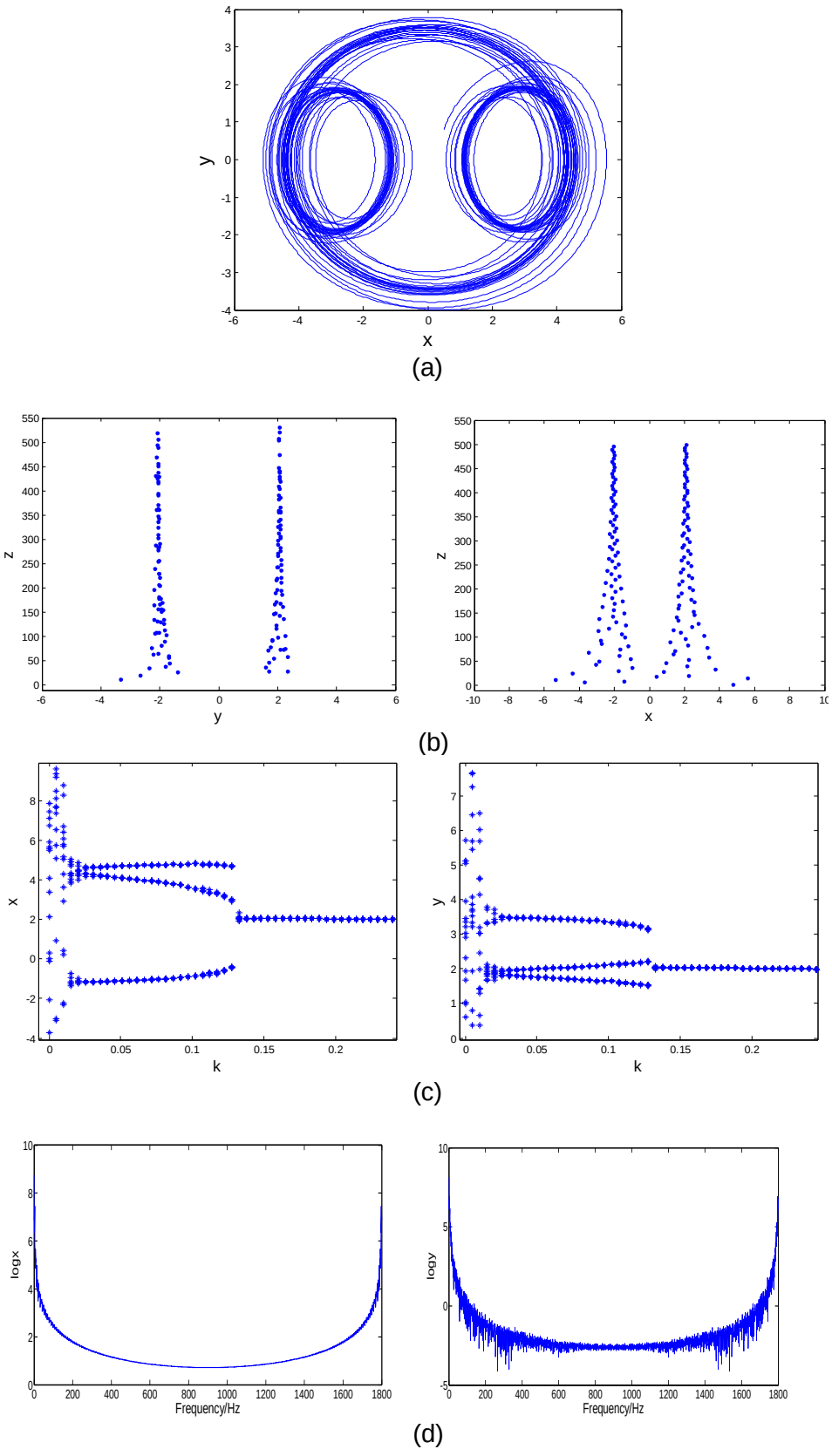

Figure 5. Simulation result obtained for Equation 11 with R=10KΩ, C=6.7μF, V_s=2p.u, ω_s=1p.u; (a) Dynamic trajectories (x-y) (b) Poincaré maps (c) bifurcation maps w.r.t k, (d) power spectrum: *logx-frequency/Hz* and *logy-frequency/Hz*.

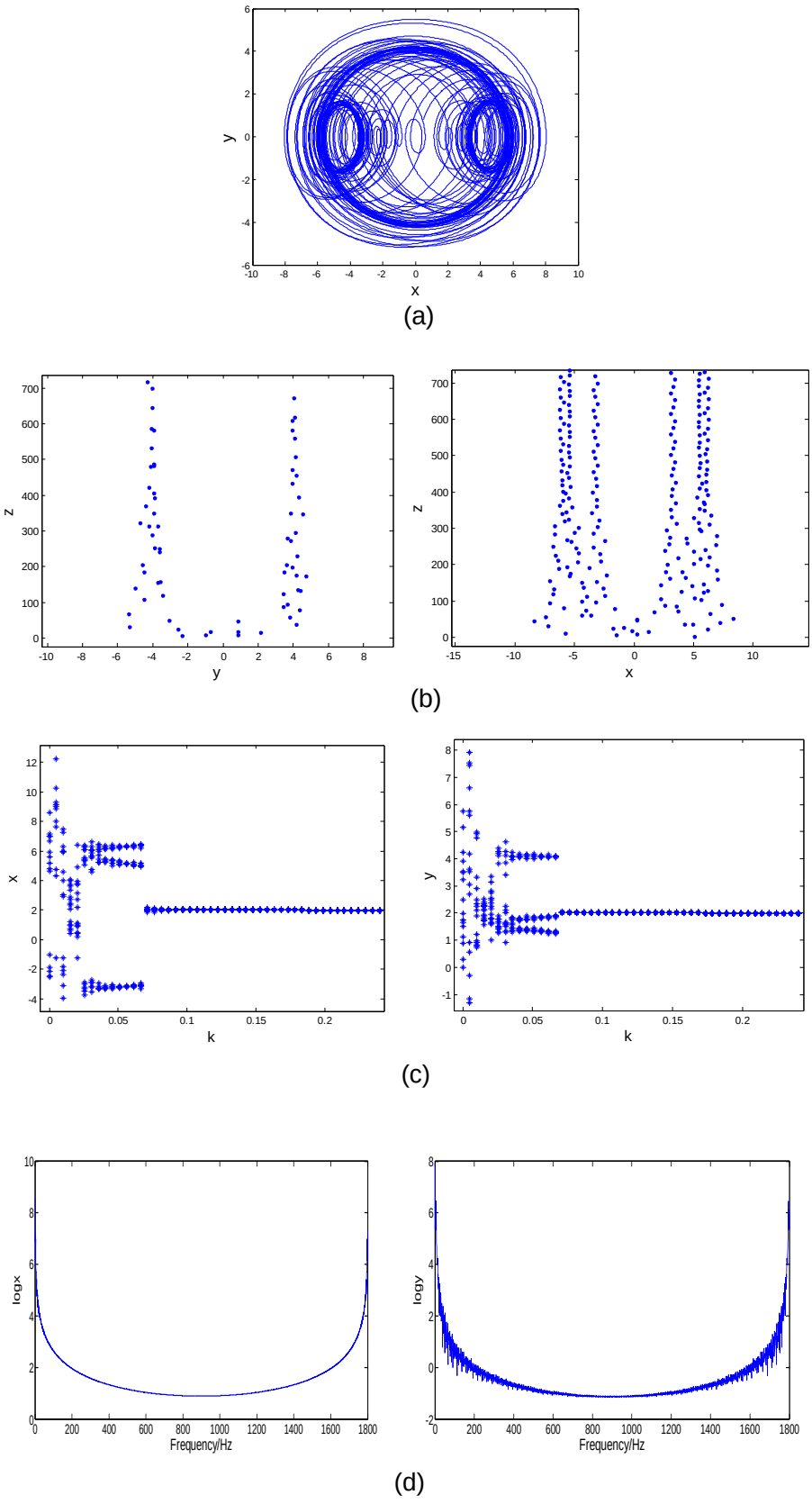

Figure 6. Simulation result obtained for Equation 11 with R=10KΩ, C=12.7μF, V_s=2p.u, ω_s=1p.u; (a) Dynamic trajectories (x-y) (b) Poincaré maps (c) bifurcation maps w.r.t k, (d) power spectrum: *logx-frequency/Hz* and *logy-frequency/Hz*.

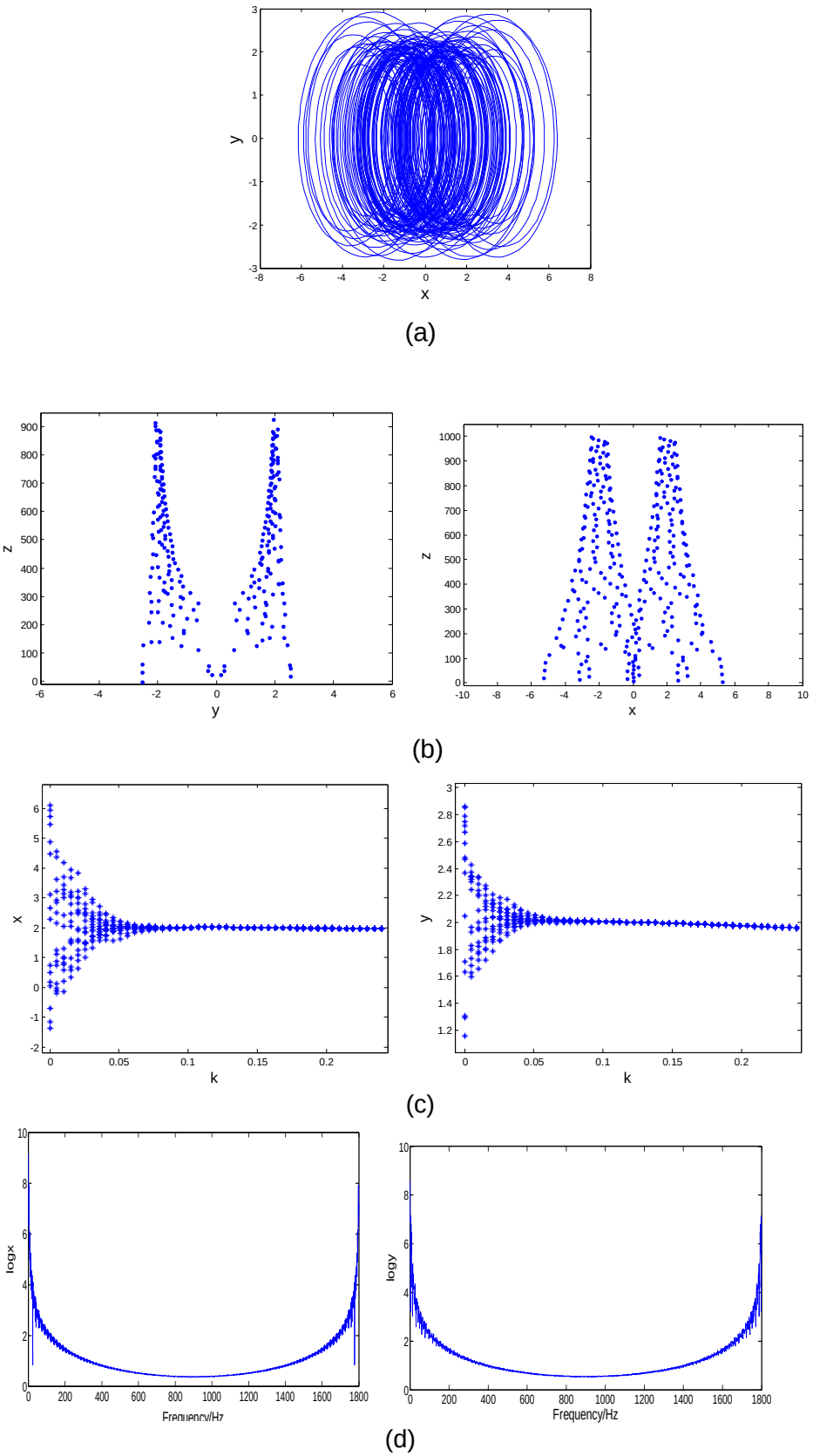

Figure 7. Simulation result obtained for Equation 11 with R=10KΩ, C=22μF, V_s=2p.u, ω_s=1p.u; (a) Dynamic trajectories (x-y) (b) Poincaré maps (c) bifurcation maps w.r.t k, (d) power spectrum: *logx-frequency/Hz* and *logy-frequency/Hz*.

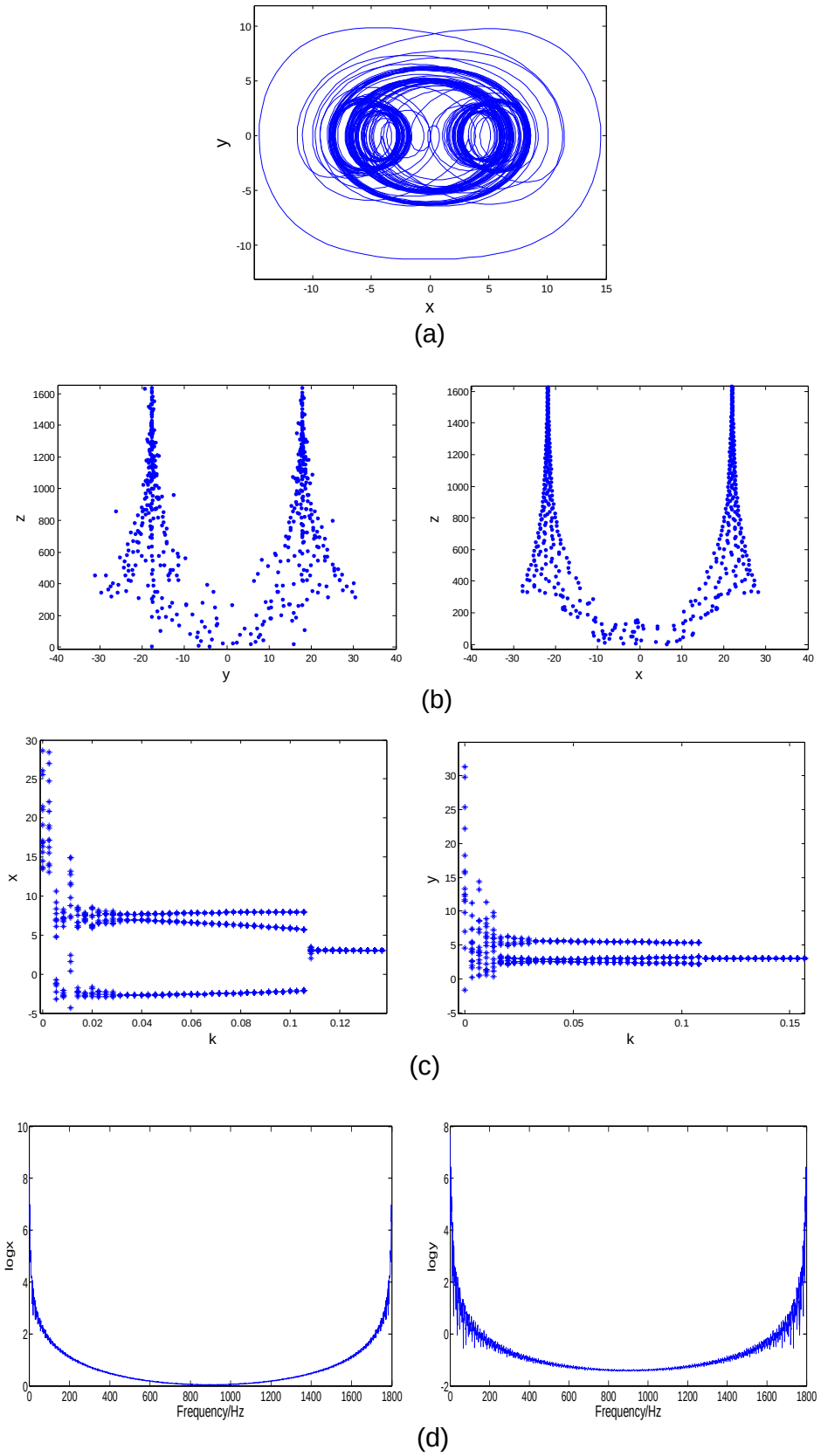

Figure 8. Simulation result obtained for Equation 11 with R=10KΩ, C=18μF, V_s=3p.u, ω_s=1p.u; (a) Dynamic trajectories (x-y) (b) Poincaré maps (c) bifurcation maps w.r.t k, (d) power spectrum: *logx-frequency/Hz* and *logy-frequency/Hz*.

$$\dot{r}=\begin{cases}\rho(|s|+\eta s^2), & |s|>\varepsilon\\ 0, & |s|>\varepsilon\end{cases} \quad (16)$$

$$s=e^{(n)}+c_1e^{(n-1)}+\cdots+c_ne \quad (17)$$

Where: e is thacking error, $e=x_d-x_1$; $m,\rho,\eta,\varepsilon>0; m\geq\eta$; m has a positive effect to the convergence rate of the controlled system, ρ and η are learning rates, ε is thacking error limits. $sat(\frac{s}{\varepsilon})=\begin{cases}sign(s), |s|>\varepsilon\\ \frac{s}{\varepsilon}, |s|\leq\varepsilon\end{cases}$; c_i meets the following equation

$$w^n+c_1w^{n-1}+\cdots+c_n=\prod_{i=1}^{n}(w+\lambda_i), \quad (18)$$

where $\lambda_1,\lambda_2,\cdots,\lambda_n$ is positive and different from each other. $\lambda_1,\lambda_2,\cdots,\lambda_n$ have a positive effect to the convergence rate.

Theorem 1: For any given $\forall t>T$, the controller Equation 15 makes Equation 14 meet the following equations.

$$\begin{aligned}&|s(t)|\leq\varepsilon\\ &|x-x_d|\leq\frac{2\|R\|\cdot\|R^{-1}\|}{\alpha}\varepsilon\end{aligned} \quad (19)$$

Where, $\alpha=\min\{\lambda_1,\lambda_2,\cdots,\lambda_n\}$ (20)

$$R=\begin{bmatrix}1 & 1 & 1 & \cdots & 1\\ \lambda_1 & \lambda_2 & \lambda_3 & \cdots & \lambda_n\\ \lambda_1^2 & \lambda_2^2 & \lambda_3^2 & \cdots & \lambda_n^2\\ \cdots & \cdots & \cdots & \cdots & \cdots\\ \lambda_1^{n-1} & \lambda_2^{n-1} & \lambda_3^{n-1} & \cdots & \lambda_n^{n-1}\end{bmatrix} \quad (21)$$

Proof: From Equation 14 and $e=x_d-x_1$, one gets

$$e^{(n)}=x_d{}^{(n)}-f(t,[x,y]^T)-u \quad (22)$$

Substitute Equation 22 into Equation 17, one getting

$$s=x_d^{(n)}+\sum_{i=1}^{n}c_ie^{(n-i)}-f(t,[x,y]^T)-u \quad (23)$$

Substitute Equation 15 into Equation 23, one getting

$$s=\int_0^t rsat(\frac{s}{\varepsilon})dt+m\int_0^t rsdt \quad (24)$$

Obviously,

$$\dot{s}=-rsat(\frac{s}{\varepsilon})-mrs \quad (25)$$

The Lyapunov function of the system is constructed as $V=0.5S^2$, and then its first derivative with respect to time is

$$\dot{V}=s\dot{s}=s\cdot[-rsat(\frac{s}{\varepsilon})-mrs]=-r[ssat(\frac{s}{\varepsilon})+ms^2] \quad (26)$$

If $|s|>\varepsilon$,

$$s\cdot sat(s/\varepsilon)=|s| \quad (27)$$

$$\dot{V}=-r(|s|+ms^2)<0 \quad (28)$$

One gets, for finite time T_1,

$$|s(t)|\leq\varepsilon, \qquad \forall t>T_1 \quad (29)$$

Now, define

$$A=\begin{bmatrix}0 & 1 & 0 & \cdots & 0\\ 0 & 0 & 1 & \cdots & 0\\ \vdots & \vdots & \vdots & \ddots & \vdots\\ 0 & 0 & 0 & \cdots & 1\\ -c_n & -c_{n-1} & -c_{n-2} & \cdots & -c_1\end{bmatrix} \quad (30)$$

$$\tilde{E}(t)=[e(t),\dot{e}(t),\cdots,e^{(n-1)}(t)]^T \quad (31)$$

$$\tilde{s}(t)=[\underbrace{0,0,\cdots,0}_{n-1},s(t)]^T \quad (32)$$

According to Equation 28, Equation 17 is rewritten as

$$\dot{\tilde{E}}(t)=A\tilde{E}(t)+\tilde{s}(t) \quad (33)$$

The solution of Equation 33 is

$$\tilde{E}(t)=e^{A(t-T_1)}\tilde{E}(T_1)+\int_{T_1}^{t}e^{A(t-\tau)}\tilde{s}(\tau)d\tau \quad (35)$$

From Equation 18, 21 and 30, Vandermonde matrix *R* meet the following equation

$$A=Rdiag\{\lambda_1,\lambda_2,\cdots,\lambda_n\}R^{-1},$$

Thus

$$e^{A(t-\tau)}=Rdiag\{e^{-\lambda_1(t-\tau)},\cdots,e^{-\lambda_n(t-\tau)}\}R^{-1} \quad (36)$$

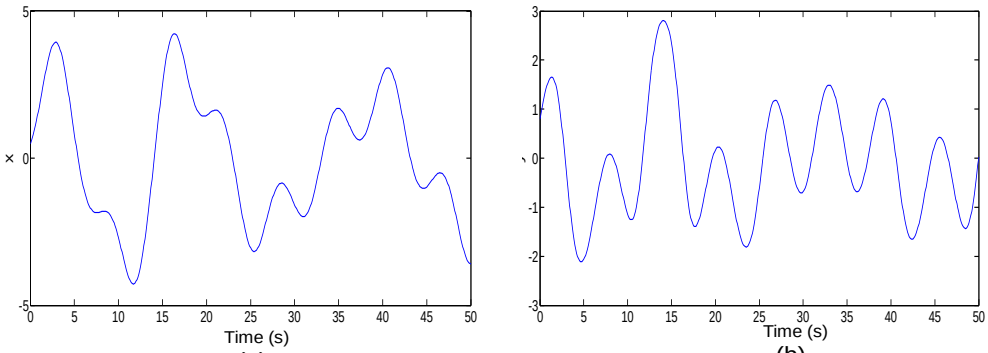

Figure 9. State responses of the Equation 35 when the control *u*(t) is not activated; (a) *x*-*t* (b) *y*-*t*.

$$\left\|e^{A(t-\tau)}\right\| = \|R\| \cdot \left\|diag\{e^{-\lambda_1(t-\tau)}, \cdots, e^{-\lambda_n(t-\tau)}\}\right\| \cdot \left\|R^{-1}\right\| \le \delta e^{-\alpha(t-\tau)} \quad (37)$$

where, $\delta = \|R\| \cdot \left\|R^{-1}\right\|$.

From Equations 40, 37 and 29, one gets

$\forall t > T_1$,

$$\left\|\tilde{E}(t)\right\| \le \left\|e^{A(t-T_1)}\right\| \cdot \left\|\tilde{E}(T_1)\right\| + \int_{T_1}^{t} \left\|e^{A(t-\tau)}\right\| \left\|\tilde{s}(\tau)\right\| d\tau \le \delta \left\|\tilde{E}(T_1)\right\| e^{-\alpha(t-T_1)} + \varepsilon \int_{T_1}^{t} e^{-\alpha(t-T_1)} d\tau$$

Thus

$$\forall t > T_1, \ \left\|\tilde{E}(t)\right\| \le \frac{\delta\varepsilon}{\alpha} + (\delta \left\|\tilde{E}(T_1)\right\| - \frac{\delta\varepsilon}{\alpha}) e^{-\alpha(t-T_1)} \quad (38)$$

Since $e^{-\alpha(t-T_1)}$ will decay to arbitrarily small in a finite time, for $T > T_1$, we have

$$\left\|\tilde{E}(t)\right\| \le \frac{2\delta\varepsilon}{\alpha} \qquad \forall t > T \quad (39)$$

Thus

$$\forall t > T, \qquad |e(t)| \le \left\|\tilde{E}(t)\right\| \le \frac{2\delta\varepsilon}{\alpha}.$$

The proof is completed.

Numerical results

The controlled form of Equation 14 is described as:

$$\begin{cases} \dfrac{dx}{dt} = y \\ \dfrac{dy}{dt} = p_1 y + p_2 x + p_3 x^3 + V_s \omega_s \cos(\omega_s t) + u \end{cases} \quad (40)$$

Where p_1=-0.0244, p_2=-0.0073, p_3=-0.0146, ω_s=1.0 and V_s=1.0.

Setting $\varepsilon = 0.001$, $\lambda_1 = 1$, $\lambda_2 = 2$, $m = \rho = \eta = 1$, $r(0) = 0.01$, c1=3, c2=2, controller *u* is designed as

$$u = -p_1 y - p_2 x - p_3 x^3 - V_s \omega_s \cos(\omega_s t) + x_d^{(2)} + \sum_{i=1}^{2} c_i e^{(2-i)} + \int_0^t rsat(\frac{S}{\varepsilon}) dt + \int_0^t rsdt \quad (41)$$

$$\dot{r} = \begin{cases} (|s| + s^2), & |s| > 0.001 \\ 0, & |s| > 0.001 \end{cases} \quad (42)$$

Fourth order Runge-Kutta integration method is used to numerical simulate the time step size (0.01) and the simulation results are carried out with initial value $[x\ y]^T=[0.5\ \ 0.8]^T$. The state responses of the Equation 40 with *u*=0 are shown in Figure 9. And it should be noticed that the controller is applied at *t*=10. The expected trajectory x_d is chosen as a fixed point x_d =0 and a periodic orbit x_d =sin(1.1t). For x_d =0, the system state responses of the closed loop system in the presence of the control law (Equation 36) are shown in Figure 10. And for x_d =sin(1.1t), the system state responses and tracking error response are shown in Figure 11. The time response of the sliding controllers is shown in Figure 12. The time response of the sliding surface is shown in Figure 13. One can clearly observe that the controller has compelled the system states onto the sliding plane and kept the states on the surface for all subsequent time. In other word, from the simulation results, it shows that the obtained theoretic results are feasible and efficient for controlling the induction motor system.

CONCLUSION

In this paper, a non-autonomous system model for third order sub-harmonic in a basic ferroresonant circuit is described. The nonlinear dynamics of the system are analyzed using dynamical trajectories, Poincaré map,

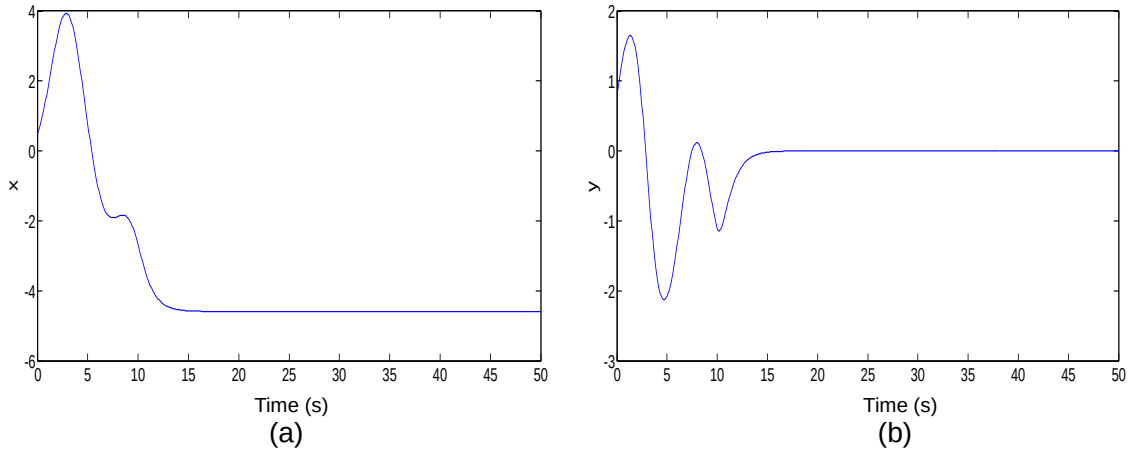

Figure 10. Time response of controlled Equation 35 when the controller u(t) is activated at t=10s, for fixed point x_d =0; (a) x-t (b) y-t.

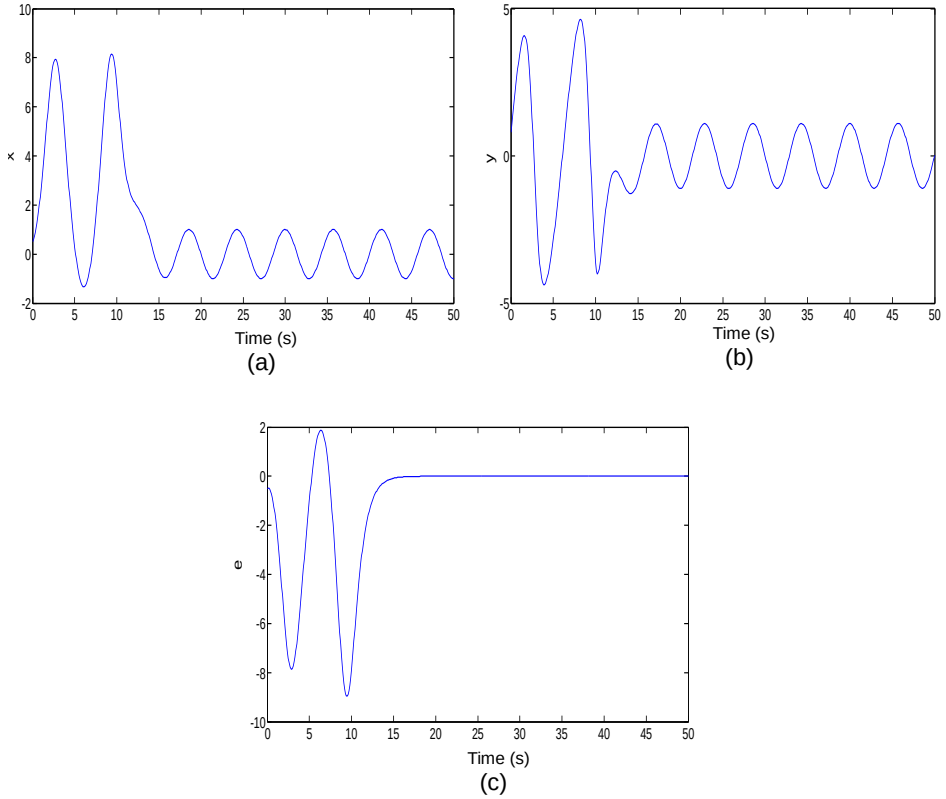

Figure 11. Time response of controlled Equation 35 and tracking error response when the controller u(t) is activated at t=10s, for fixed point x_d =sin(1.1t); (a) x-t (b) y-t.

bifurcation diagram, dissipativity analysis and spectrogram map. Numerical simulation result shows chaotic motion. Then we design a sliding mode controller with only one term for the chaotic system, which is no-chatting for its saturation function. Thus, the control method can guarantee the stability and reliability of the system. Both theory analysis and numerical simulation result are presented to demonstrate the validity of the proposed control.

Future research may focus on the following topics. Firstly, new dynamical behaviors for nonlinear systems need to be discovered. And the relationship of complex dynamical characters could be discussed with each other. Secondly, new controlling method should be studied,

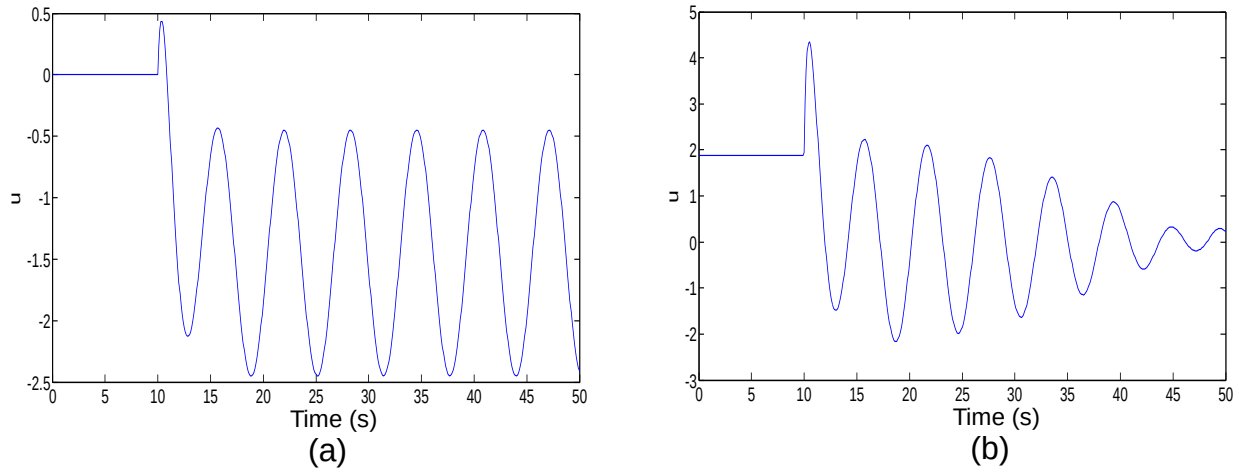

Figure 12. The time response of the controller $u(t)$ which is activated at t=10s; (a) *For* x_d =0 (b) *For* x_d =sin(1.1t).

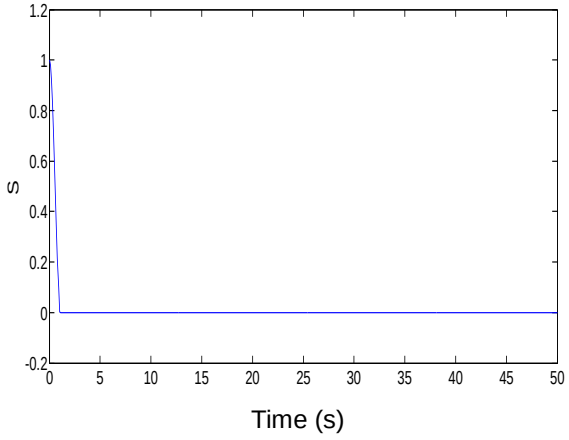

Figure 13. The time response of the sliding surface

which is suitable for uncertainties, external disturbances, unknown parameters and input nonlinearities.

Nomenclature: V_s, Peak value of the sinusoidal supply voltage; ω_s, angular frequency of the supply voltage; C, coupling capacitance; R, transformer shunt resistance representing core loss; λ, Flux linkage in the nonlinear inductor; i_M, magnetizing current; a, Coefficient of the linear part of magnetization characteristics; b, coefficient of the nonlinear part of magnetization characteristics; n, exponent corresponding to the nonlinear magnetization characteristics; ω_0, Natural frequency of the ferroresonant circuit.

REFERENCES

Barbisio E, Bottauscio O, Chiampi M, Crotti G, Giordano D (2007). Experimental and modelling analysis of ferroresonant electric circuits. J. Magn. Magn. Mater., 316: E299-E301.

Ben Amar F, Dhifaoui R (2011). Study of the periodic ferroresonance in the electrical power networks by bifurcation diagrams. Int. J. Elect., 33: 61-85.

Brandt ME, Chen G (1997). Bifurcation control of two nonlinear models of cardiac activity. IEEE T. Circuits, 44: 1031-1034.

Chen DY, Shen T, Ma XY (2011b). Sliding mode control of chaotic vibrations of spinning disks with uncertain parameter under bounded disturbance. Acta Phys. Sin., 60: 050505. (In Chinese).

Chen DY, Wu C, Liu CF, Ma XY, You YJ, Zhang RF (2012). Synchronization and circuit simulation of a new double-wing chaos. Nonlin. Dyn., 67: 893-901.

Chen DY, Zhao WL, Ma XY, Zhang RF (2011a). No-chattering sliding mode control chaos in Hindmarsh-Rose neurons with uncertain parameters. Comput. Math., 61: 3161-3171.

Henning AJ, Fromhold TM, Wilkinson PB (2011). Using dynamical barriers to control the transmission of light through slowly varying photonic crystals. Phys. Rev. E., 83: 046209

Hui M, Zhang YB, Liu CX (2009). Analysis of ferroresonance in a neutral grounding system with nonlinear core loss. Chin. Phys. B., 18: 1787-1791.

Jacobson DAN, Lehn PW, Menzies RW (2002). Stability domain calculations of period-1 ferroresonance in a nonlinear resonant circuit. IEEE Trans. Power Deliv., 17: 865-871.

Jacobson DAN, Lehn PW, Menzies RW (2002). Stability domian calculations of period-1 ferroresonance in a nonlinear resonant circuit. IEEE T. Power Deliv., 17: 865–71.

Kavasseri RG (2006). Analysis of sub-harmonic oscillations in a ferroresonant circuit. Int. J. Elec. Power, 28: 207-214

Khadra A, Liu XZ, Shen X (2005). Impulsively synchronizing chaotic systems with delay and applications to secure communication. Automatica, 41: 1491-1502.

Lamba H, Mckee S, Simpson R (1998). The effect of circuit parameters on ferroresonant solutions in an LCR circuit. J. Phys. A-Math. Theor., 31: 7065-7076.

Lind MGJ, Xiao WD, Dunford WG (2006). Modeling of a constant voltage transformer. IEEE T. Circuits, 53: 409-418.

Liu YJ, Yang QG (2010). Dynamics of a new Lorenz-like chaotic system. Nonlin. Anal. Real, 11: 2563-2572.

Ma J, Wang CN, Tang J, Xia YF (2009). Suppression of the spiral wave and turbulence in the excitability-modulated media. Int. J. Theor. Phys., 48: 150–157.

Milicevic K, Lukacevic I, Flegar I (2009). Modeling of nonlinear coil in a ferroresonant circuit. Electr. Eng., 91: 51-59.

Milicevic K, Pelin D, Flegar I (2008). Measurement system for model verification of non autonomous second-order nonlinear systems. Chaos Soliton Fract., 38: 939-948.

Mozaffari S, Henschel S, Soudack AC (1995). Chaotic ferroresonance in power transformers. IET Gener. Transm. Distrib., 142: 247–50.
Nayfeh AH (1981). Introduction to perturbation techniques. Wiley, London.
Nayfeh AH, Mook DT (1979). Nonlinear oscillations. Wiley, London.
Paula de AS, Savi MA (2009). A multiparameter chaos control method based on OGY approach. Chaos Soliton Fract., 40: 1376-1390.
Preetham KS, Saravanaselvan R, Ramanujam R (2006). Investigation of subharmonic ferroresonant oscillations in power systems. Electr. Power Compon. Syst., 76: 873-879
Preetham KS, Saravanaselvan R, Ramanujam R (2006). Investigation of subharmonic ferroresonant oscillations in power systems. Electr. Power Syst. Res., 76: 873-879.
Saravanaselvan R, Ramanujam R (2011). Detection and analysis of isolated subharmonic ferroresonant solutions in power transformers. Eur. T. Electr. Power, 21: 82-88.
Schiff SJ, Jerger K, Duong DH, Chang T, Spano ML, Ditto WL (1994). Controlling chaos in the brain. Nature, 370: 615-620.
Shi P, Xia Y, Liu G, Rees D (2006). On designing of sliding mode control for stochastic jump systems. IEEE T. Automat. Contr., 51: 97-103.
Wang H, Han ZZ, Zhang W, Xie QY (2009). Synchronization of unified chaotic systems with uncertain parameters based on the CLF. Nonlin. Anal. Real, 10: 715-722.
Wang JW, Ma QH, Zeng L, Abd-Elouahab MS (2011). Mixed outer synchronization of coupled complex networks with time-varying coupling delay. Chaos, 21: 013121.
Wornle F, Harrison DK, Zhou C (2005). Estimation of the model parameters of ferroresonant circuits using jump voltage assignment. IEE Proceedings-Circuits Dev. Syst., 152: 76-82.
Wornle F, Harrison DK, Zhou CK (2005). Analysis of a ferroresonant circuit using bifurcation theory and continuation techniques. IEEE Transactions on Power Deliv., 20: 191-196.
Yokoi Y, Hikihara T (2011). Tolerance of start-up control of rotation in parametric pendulum by delayed feedback. Phys. Lett. A., 375: 1779-1783.
Zhang J, Small M (2006). Complex network from pseudoperiodic time series: Topology versus dynamics. Phys. Rev. Lett., 96: 238701.
Zhang J, Zhang K, Feng JF, Small M (2010). Rhythmic Dynamics and Synchronization via Dimensionality Reduction: Application to Human Gait. PLoS Comput. Biol., 6: e1001033.